

An enhanced differential evolution-based inverse radiation transport model for identification of unknown shielding layer thicknesses with gamma-ray spectrum

Ying Chen¹ · Lian-Ping Zhang¹ · Xue Sai² · Meng-Fu Wei¹ · Lun-Qiang Wu¹ · Jian-Min Hu¹

Received: 28 June 2016/Revised: 10 August 2016/Accepted: 7 October 2016/Published online: 6 May 2017
© Shanghai Institute of Applied Physics, Chinese Academy of Sciences, Chinese Nuclear Society, Science Press China and Springer Science+Business Media Singapore 2017

Abstract Identifying the geometric information of an object by analyzing the detected radiation fields is an important problem for national and global security. In the present work, an inverse radiation transport model, based on the enhanced differential evolution algorithm with global and local neighborhoods (IRT-DEGL), is developed to estimate the unknown layer thickness of the source/shield system with the gamma-ray spectrum. The framework is briefly introduced with the emphasis on handling the enhanced differential evolution algorithm. Using the simulated gamma-ray spectra, the numerical precision of the IRT-DEGL model is evaluated for one-dimensional source systems. Using the detected gamma-ray spectra, the inverse investigations for the unknown thicknesses of multiple shielding layers are performed. By comparing with the traditional gamma-ray absorption method, it is shown that the IRT-EDGL model can provide a much more accurate result and has great potential to be applied for the complicated systems.

Keywords Inverse radiation transport · γ Spectrometry · Multi-shielding layers · Differential evolution with local and global neighborhoods

This work was supported by the CAEP foundation for Development of Science and Technology (No. 2015B0103014) and National Natural Science Foundation of China (No. 11605163).

✉ Ying Chen
cyingecho@caep.cn

¹ Institute of Materials, China Academy of Engineering Physics, Jianguo, Mianyang 621907, China

² Science and Technology on Surface Physics and Chemistry Laboratory, Mianyang 621908, China

1 Introduction

Techniques acquiring the special and geometric information for an object by analyzing the detected radiation fields, which is usually classified as inverse radiation problem, play an important role in the applications that support nonproliferation, arms control verification and international security. During the past decades, great efforts have been dedicated to studying the roles of gamma-ray transports in the medium and the interaction between gamma rays and medium materials [1] and to attempting to find the solution of the inverse transport problems using either explicit method or implicit method [2].

The gamma-ray absorption method is one of the most common explicit methods used to identify the geometric information of a source/shield system with detected radiation information, for example, the thicknesses of shielding layers are obtained explicitly by analyzing the several gamma-ray intensities detected with and without shielding materials as well as the shielding material absorption properties. This method has been applied to identify the shielding material thickness several decades ago and is also one of the most popular methods nowadays for rough estimation due to its convenience [3–6]. However, the disadvantage for such explicit methods is also obvious, e.g., the gamma-ray absorption method may be unsuitable for the complicated source systems with unsymmetrical geometry characteristics as well as the source systems with multilayer shielding material where one often has to deal with the ill-conditioned equations [7].

Another possible way to identify the unknown properties of radiation source terms and transport media is the implicit method, which is called the inverse radiation

transport method here, in which the nonlinear regression is applied to the forward transport model, and the unknown source/shield properties are treated as regression variables and iteratively modified until the calculated spectrum matches the measured spectrum [2, 8]. In comparison with the explicit method, the inverse radiation transport method is more generally tractable and more general in its applications, and therefore, numerous techniques including the Levenberg–Marquardt method [7, 9], differential evolution (DE) method [10, 11] and mesh adaptive direct search (MADS) [12] method are applied to improve the inverse transport models for a variety of applications.

Among these numerical techniques, the Levenberg–Marquardt method as a standard gradient-based optimization algorithm has been used to solve the inverse problems with relatively few unknowns, approximately smaller than 4, and achieved high success with proper initial guess [8]. References [9, 10, 13] coupled the forward and adjoint radiation transport solutions to evaluate the inverse method and identify the locations of interfaces between material layers, source composition, shield material identification and material mass density, as well as the combinations of these unknown properties in spherical and cylindrical radiation source/shield system, and moreover, several numerical investigations using simulated experimental gamma-ray spectra were performed to examine the validity and precision for the inverse solver. Reference [7] adopted the numerical difference techniques instead of the adjoint solution to develop an inverse solver and applied the solver to estimate the thickness of one-dimensional plutonium metal as well as the shielding iron shell with analysis of full detected gamma-ray spectra. Later, Mattingly extended the inverse solver to simultaneously analyze gamma spectrometry and neutron multiplicity measurements [14] for the unknown layer thicknesses of one-dimensional source systems, and the experimental validation for the inverse solver is discussed [15].

Later, the differential evolution (DE) method, the mesh adaptive direct search (MADS) method and the covariance matrix adaptation evolution strategy (CMA-ES), powerful evolution optimization algorithms, have been applied to solve inverse problems for spherical geometries with uncollided leakages of discrete gamma-ray lines and for cylindrical geometries with uncollided scalar fluxes with gamma-ray lines at points outside the system [10, 12, 16], where the experimental gamma-ray spectra are obtained by simulation. It is found that numerically the inverse solver, based on the evolution optimization algorithm, can be applied for the system with unknowns more than 4 with random initial guess and achieves much higher success rate for the same inverse problem in comparison with gradient-based method, indicating that the evolution optimization algorithm is more proper for the inverse radiation transport

problems [12, 17]. Besides, it is also suggested that more algorithm improvement, as well as experimental validation and testing for such inverse solvers, is still needed.

Recently, an enhanced differential evolution algorithm with global and local neighborhoods (DEGL) has been proposed and is suggested to perform better than the standard differential evolution algorithm [18, 19]. Therefore, in the present paper, an inverse radiation transport model is developed based on DEGL (IRT-DEGL), and the numerical evaluation of the present inverse model is performed using both simulated and detected gamma-ray spectra.

2 Differential evolution enhanced with global and local neighborhoods

The differential evolution algorithm enhanced with global and local neighborhoods (DEGL) has introduced the neighborhood-based DE mutation, which is equipped with a self-adaptive weight factor, and attempts to make a balanced use of the exploration and exploitation abilities of the search mechanism. Therefore, it is thought to be more likely to avoid false or premature convergence and suggested to be attractive for optimizing a wide variety of objective functions [18, 19].

The implementation process for the inverse radiation transport model based on the DEGL algorithm is similar to that based on the standard DE method shown in Ref. [11]. In comparison with the implementation process reported in Ref. [11], the present inverse model uses the following mutation operation to create trial vectors $\mathbf{v}_i (i = 1, \dots, P)$, denoted as:

$$\mathbf{v}_i^{(h)} = \omega \cdot \mathbf{g}_i^{(h)} + (1 - \omega) \cdot \mathbf{l}_i^{(h)} \quad (1)$$

with the global neighborhood mutation $\mathbf{g}_i^{(h)}$ and local neighborhood mutation $\mathbf{l}_i^{(h)}$

$$\begin{aligned} \mathbf{g}_i^h &= \mathbf{u}_i^{(h)} + \alpha \cdot \left(\mathbf{u}_{\text{best},i}^{(h)} - \mathbf{u}_i^{(h)} \right) + \beta \cdot \left(\mathbf{u}_a^{(h)} - \mathbf{u}_b^{(h)} \right), \\ \mathbf{l}_i^h &= \mathbf{u}_i^{(h)} + \alpha \cdot \left(\mathbf{u}_{\text{pbest},i}^{(h)} - \mathbf{u}_i^{(h)} \right) + \beta \cdot \left(\mathbf{u}_c^{(h)} - \mathbf{u}_d^{(h)} \right), \end{aligned} \quad (2)$$

where the total population size, P , which is usually 3 times larger than the unknown number, is set to 9 in the present paper, the evolution generation is represented as h , and the largest generation number, h_{max} , equals 100. $\mathbf{u}_{\text{best},i}^{(h)}$ indicates the best vector in the entire population at generation h and random integral numbers $a, b \in [1, P]$ with $a \neq b \neq i$ as the scaling factors. $\mathbf{u}_{\text{pbest},i}^{(h)}$ indicates the best vector in the neighborhood of $\mathbf{u}_i^{(h)}$ with random integral numbers $c, d \in [i - k, i + k]$ with $p \neq q \neq i$, where the neighborhood of radius, k , is a nonzero integer from 0 to $(P - 1)/2$ and is

fixed to be $(P - 1)/2$ here. Scaling factors α and β are used to consider both arithmetical recombination operation and differential mutation and are set to be 0.7 in the present paper.

The weight factor, ω , controlling the balance between the exploration and exploitation capability is defined as

$$\omega = \exp\left(\frac{h}{h_{\max}} \cdot \ln 2\right) - 1.0, \tag{3}$$

which means the exploration is favored in the first stage of the algorithm's execution with $\omega = 0$ corresponding to the local neighborhood search, and the exploitation is promoted at the final stages with $\omega = 1$ corresponding to the global neighborhood search.

The cost function that represented the difference between the measured and calculated spectra is denoted as

$$f(\mathbf{u}) = \sum_g \left| \frac{R_g - R_g(\mathbf{u})}{R_g} \right|, \tag{4}$$

where R_g is the measured data, and $R_g(\mathbf{u})$ is the calculated value using postulated parameter set, \mathbf{u} . The sum over g can run over the full gamma-ray spectrum or the strong gamma emission lines large enough to include gamma-ray spectrum characteristics as much as possible.

3 Results and discussion

3.1 Simulation investigation

In order to evaluate the numerical precision of the present IRT-DEGL model, two testing spherical multilayered source/shield systems are considered first. The first source system adopted is a multilayer shield high-enriched uranium (HEU) sphere, where a HEU source (94.73% ^{235}U and 5.27% ^{238}U) of density 18.74 g/cm³ with radius 8.471 cm is at the center and surrounded by a void between 8.471 and 12.40 cm, a shielding layer of aluminum is between 12.40 and 12.90 cm, and a shielding layer of iron is between 12.90 and 13.20 cm. The second source system is a multilayer shield HEU shell with the same material compositions as the first testing model, and the geometric information can be found in Table 1. The material in each layer is homogeneous. Generally, in a real detection, one can get the accurate outer radius of a source system with various measurement techniques, while the thickness of the shielding layers is not easy to be obtained without opening the source system. Therefore, in the present investigation, we assume that the outer radius of the source system is already known, and the inverse calculations for the unknown thickness for shielding layers as well as the source radius are carried out. The modeled HPGe detector

Table 1 Thickness of the HEU source and shielding materials for the testing source/shield systems in units of cm

	HEU	Void	Aluminum	Iron
<i>Testing source/shield system I</i>				
Initial	8.200	3.800	0.600	0.600
IRT-DEGL	8.471	3.929	0.500	0.300
Actual	8.471	3.929	0.500	0.300
	Void	HEU	Aluminum	Iron
<i>Testing source/shield system II</i>				
Initial	10.000	1.000	1.000	1.200
IRT-DEGL	10.471	0.929	1.500	0.300
Actual	10.471	0.929	1.500	0.300

is 20 cm from the center of the source system, and for the simulated experimental data with Monte Carlo code MCNP5 [20], the full gamma-ray spectrum is used for the inverse calculation.

It is known that one of the advantages for the inverse transport model based on the differential evolution method is that its calculation results do not depend on the initial guesses. Therefore, one can, in principle, create the initial values for the unknown radii under the constraint given by prior information of the source system, that is, one can create a value between 0.00 and 13.20 cm for the HEU source in both testing models. However, since the different attenuation of the photopeaks and the shape of the Compton continuum associated with the photopeak are dependent on the shielding materials, it is possible to obtain the estimated values for the unknown layer thicknesses from the empirical formula and prior information, which can help to reduce the computing time greatly. In the inverse calculations for the testing source/shield systems, the initial radii are listed in Table 1, where the largest relative difference between the initial and actual values range reaches 400.0%.

After the respective 68 and 53 generation evolution, the IRT-DEGL calculations for testing source system I and II converge with the cost function of optimal vector $f(\mathbf{u}_{\text{opt}}) < 0.005$. The statistical errors of the full-energy peak areas for the four strongest energy lines of HEU are smaller than 1% in the Monte Carlo simulations. The calculated thicknesses of the HEU source, aluminum and iron shielding layers are the same with the real values up to 0.001 cm, numerically indicating that present inverse model can be applied to investigate the unknown properties of the source/shield system with high precision. Furthermore, it is worth pointing out that during the inverse calculations the relative differences between the calculated

and actual thicknesses are smaller than 0.1% after a 10-generation evolution for both testing models, and therefore, it is necessary to set up the proper stopping criteria or to stop iteration manually according to the actual precision requirement.

3.2 Experimental investigation

In order to evaluate the present IRT-DEGL model and study the influence of using the detected gamma-ray spectra for the shielding layer thickness estimation, a series of experiments for the source/shield systems are conducted with a 60% relative efficiency HPGe spectrometer.

It is known that the precise full-energy peak efficiency calibration of HPGe detectors for the wide energy range is important in gamma-ray spectrometry, especially for the quantitative investigations of the source systems with unknowns. As we know, the thickness of the dead layer of HPGe detector crystals may vary considerably with the time, and the detection efficiency estimated by Monte Carlo simulation with the manufacturer's value usually has a significant discrepancy from the experimental measurement [21, 22]. One of the possible methods to overcome this difficulty is to vary the thickness of the dead layer in the simulation until a good agreement between the simulation and experiment is reached with a suitable thickness. Thus, before the inverse investigations, the full-energy peak efficiency calibration for the HPGe detector we used is performed with a point source ^{152}Eu .

In Fig. 1, the relative efficiencies, the efficiency related to the strongest 122 keV energy line, simulated with the manufacturer's dead layer thickness, 0.7 mm, and optimized value, 0.8 mm, for the energy lines ranging from 0.1 to 1.4 MeV in comparison with the experimental data are shown in the panel (a), and the relative differences between the simulated and experimental values are plotted in panel (b). The statistical errors of the full-energy peak areas for these energy lines are smaller than 1% in both experimental data and simulated values. One can see that both simulated and experimental values decrease with increasing energy. The simulation results obtained with the manufacturer's dead layer thickness of 0.7 mm are systematically higher than the experimental data with the relative differences almost larger than 3%, indicating that the manufacturer's value is smaller than the real thickness. Therefore, we increase the thickness by every 0.05 mm and find that when the thickness of dead layer equals 0.8 mm, the simulated results achieve good agreement with the detected data. The relative difference is smaller than 3% for most energy lines, which is reduced by half in comparison with the values obtained with 0.7 mm. Therefore, the dead layer thickness of 0.8 mm is fixed in the present paper.

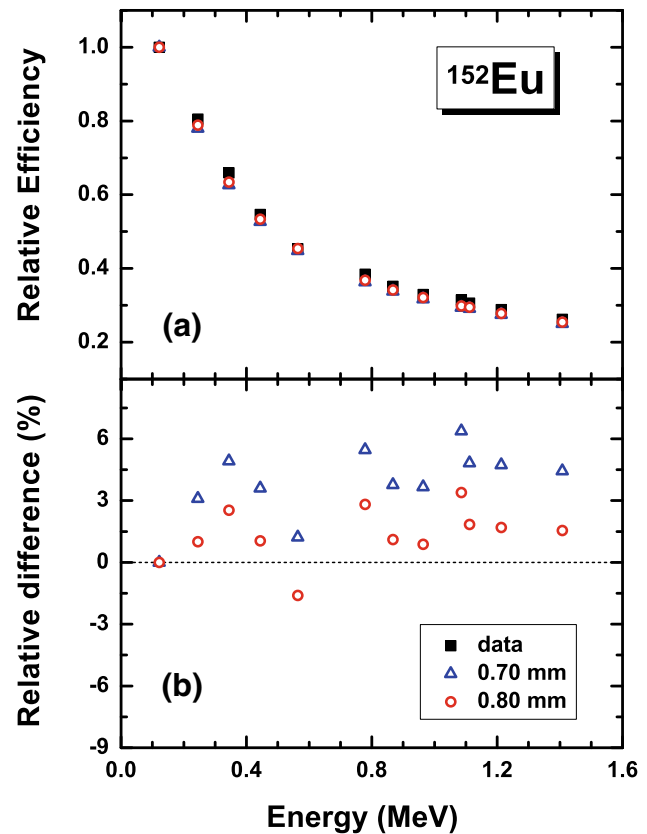


Fig. 1 (Color online) Relative efficiency obtained with the dead layer thickness 0.7 mm given by manufacture and 0.8 mm optimized in comparison with the experimental data in panel (a), as well as the corresponding relative differences between the simulated and detected values in panel (b)

Actually, it should be pointed out that there are also some other reasons for the introduction of the error into the simulation of full peak detection efficiencies, e.g., the distance between the radiation source and the surface of detector, the gap between the HPGe detector crystal and Al shell, and the position of HPGe detector crystal. The optimization for the dead layer thickness of crystal is not only to correct the detector geometry, that is, the optimized thickness of dead layer is not absolute to the actual thickness than the manufacturer's value, but also to provide an effective compensation for the thickness of the dead layer as well as other effects which can influence the detection efficiency but are not included in the simulation calculations. If a more accurate simulation result is required, a more precise optimization for dead layer thickness as well as the further optimization of crystal parameters, e.g., size and cold finger, can be performed.

To establish the present IRT-DEGL model experimentally, a simple example is adopted for the first attempt, where a shielding layer of copper with a thickness of 0.308 cm is located between the point source ^{152}Eu and the HPGe detector. The detection situation is the same as the one for

detector efficiency calibration except for the copper shielding layer. The thickness of the copper layer is assumed to be unknown. The density of the copper layer equals 8.96 g/cm^3 , and the material in the layer is homogeneous. The distances between the source and the HPGe detector, and between one surface of copper layer and the detector are already known. The measurements of the full-energy peak area for the strong emission lines adopted in HPGe detector efficiency calibration are used. The statistical errors for both experimental and simulated full-energy peak areas for these emission lines are smaller than 1%.

In Fig. 2, the cost function of the optimal parameter set $f(\mathbf{u}_{\text{opt.}})$ as well as the optimal thickness of copper layer estimated in each generation are shown. The 0 generation denotes the results obtained with the initial thickness set to be 1.5 cm which is about 5 times larger than the real values. It can be seen that the cost function of the optimal parameter set decreases with the increasing generation monotonically, especially for the 0 to 1 generation; the value of the cost function is reduced from 29.3 to 2.19% and becomes smaller than 1.0% for only 4 generations of

evolution, indicating that the present inverse radiation transport model can search the area around the actual value rapidly. If one just needs the rough thickness value, then the iteration calculation can be stopped manually, and a thickness of 2.86 cm is obtained. Here, since the aim is to test the numerical precision with the experimental gamma-ray spectrum, the iteration calculation is set to continue until the cost function $f(\mathbf{u}_{\text{opt.}})$ is smaller than 0.5% and does not decrease for 5 generations. After 11 generations, the inverse calculation stops with the cost function $f(\mathbf{u}_{\text{opt.}}) = 0.02\%$, and the optimal thickness of copper layer equals 0.313 cm with the relative difference 1.62% from actual value.

Of course, one can also use the traditional gamma-ray absorption method to estimate the unknown layer thickness by analyzing the relative intensity for several gamma rays detected with and without the shielding layer exactly, i.e.,

$$r = \frac{\ln A_0 - \ln A}{\mu(E_i) - \mu(E_j)} \tag{5}$$

with

$$A_0 = \frac{I_0(E_i)}{I_0(E_j)}, \quad A = \frac{I(E_i)}{I(E_j)}, \tag{6}$$

where r denotes the thickness of the copper layer, $I_0(E_i)$ and $I(E_i)$ denote the intensity of the E_i line detected without and with the copper layer, respectively, and $\mu(E_i)$ denotes the absorption coefficient of copper for the E_i line. In the present paper, the difference $\delta\mu = (\mu(E_i) - \mu(E_j))$ is calculated for the strongest 122 and 244 keV lines in the Monte Carlo simulation and is shown in Table 2, where several thicknesses of copper layer are considered. It is shown that the simulated results with different assumed thicknesses are consistent with each other and the values are around 1.5 cm^{-1} .

Using the simulated absorption coefficient differences, $\delta\mu$, the thickness of the copper layer is solved with Eq. 5 and is shown in Table 3 in comparison with the IRT-DEGL result. The results from the gamma-ray absorption method are the same with each other up to 0.01 cm with the relative differences from the actual value around 5%, which is about 2 times larger than the inverse calculation result. This is because in the gamma-ray absorption method only

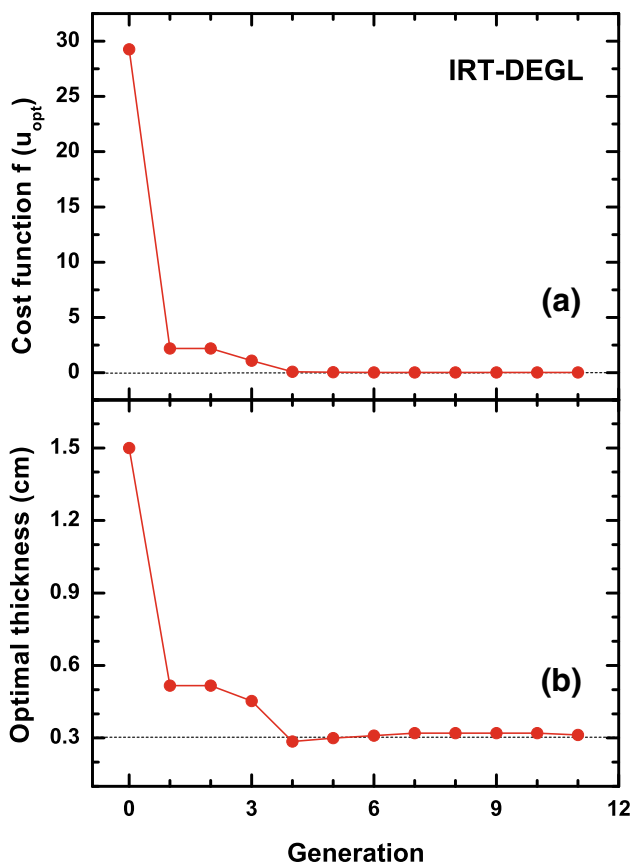


Fig. 2 (Color online) The cost function of optimal parameter set $f(\mathbf{u}_{\text{opt.}})$, **a** as well as the corresponding optimal thickness of copper layer estimated in each generation, **b** is shown as a function of generation number. The dotted line denotes the zero value in panel (a) and actual thickness of copper layer in panel (b)

Table 2 Differences between the absorption coefficients $\delta\mu = (\mu(E_i) - \mu(E_j))$ for the 122 and 244 keV lines obtained by the Monte Carlo simulation with different copper layer thicknesses

	Monte Carlo simulation results		
	0.200 (cm)	0.300 (cm)	0.500 (cm)
$\delta\mu \text{ (cm}^{-1}\text{)}$	1.506	1.489	1.463

Table 3 Comparison between the results from the gamma-ray absorption method using the values of $\delta\mu$ shown in Table 2 and the IRT-DEGL model

r (cm)	Absorption method			IRT-DEGL model
	0.286	0.289	0.294	
$ \delta r/r $	7.14%	6.17%	4.55%	1.62%

two energy lines are used to estimate the layer thickness, while in the inverse radiation transport model the consideration of 11 full-energy peaks allowed us to analyze enough characteristics of the gamma-ray spectrum and obtain the more accurate results. Furthermore, in the gamma-ray absorption method the additional treatment of the absorption coefficient and the detected spectrum without shielding layer may also introduce more numerical errors.

For further establishing the present IRT-DEGL model, we added one more layer of aluminum with a thickness of 0.570 cm into the previous detection system already including one copper layer and detected the gamma-ray spectrum for the inverse study. Considering the cases in which the shielding layers are encapsulated as a whole, it is not easy to distinguish the layer thicknesses easily. The thicknesses of the copper layer and aluminum layer are both assumed to be unknown. The densities of the copper layer and aluminum layer are 8.96 and 2.7 g/cm³, respectively, and the material in the layer is homogeneous. Two layers are close to each other, and the copper layer is on the side closest to the HPGe detector. The distance between the radiation source and HPGe detector and the distance between the HPGe detector and one surface of the copper layer are already known. Also, the statistical errors for both experimental and simulated full-energy peak areas for these emission lines are smaller than 1%.

The IRT-DEGL calculation is performed using the initial guesses of 0.5 cm for the copper layer and 0.7 cm for the aluminum layer with the detected full-energy peak areas of the 7 strongest emission lines of ¹⁵²Eu (122, 344, 779, 964, 1086, 1112 and 1408 keV). The optimal thicknesses for the copper layer and aluminum layer in each generation are plotted in Fig. 3, and the actual values are represented as dotted lines. The 0 generation denotes the initial thicknesses. It can be also seen that the after 1 generation the estimated thicknesses for the copper layer are located in the area around the actual values, indicating the present IRT-DEGL model can search the correct value area rapidly. After 19 generations of evolution, inverse calculation stops because the cost function, $f(\mathbf{u}_{opt.})$, does not change for 5 generations. The final optimal thicknesses of the copper layer and aluminum layer are 0.319 and 0.531

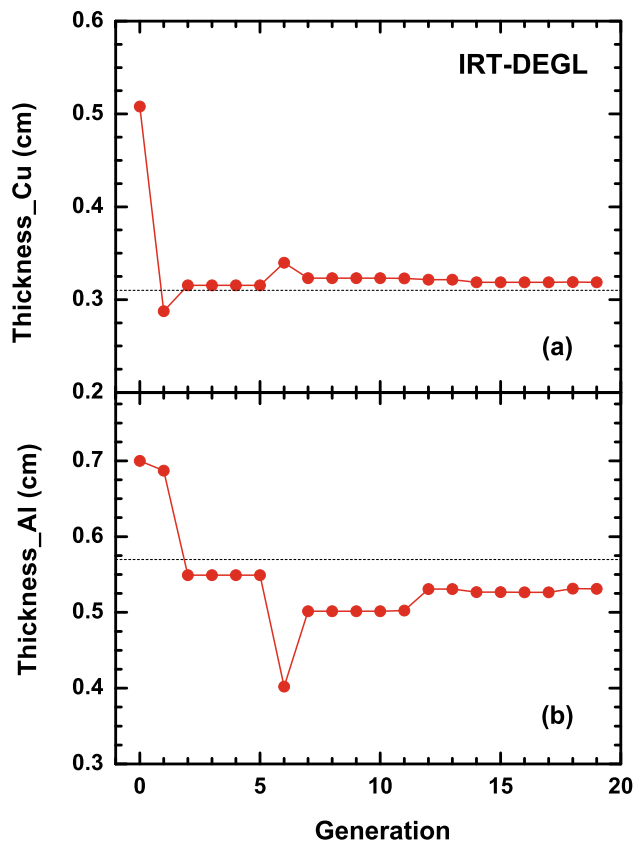


Fig. 3 (Color online) Optimal thicknesses for copper layer (a), aluminum layer (b) estimated by the IRT-DEGL model as a function of generation. The dotted line denotes actual thicknesses of copper and aluminum layers

cm corresponding to the relative differences from the actual value 3.57 and 6.84%, respectively. The major reasons for the deviation may include the statistical error and extracting error for the experimental full-energy peak area, theoretical simulation of the HPGe detector and detection process, and lack of enough spectrum characteristics to be analyzed in inverse calculation.

Again, the gamma-ray absorption method is used to calculate the unknown layer thicknesses for comparison. Analyzing the intensity of the gamma ray transporting with and without shielding layer, one can construct the following equation,

$$\begin{pmatrix} -\mu_{r_1}(E_i) + \mu_{r_1}(E_j) & -\mu_{r_2}(E_i) + \mu_{r_2}(E_j) \\ -\mu_{r_1}(E_k) + \mu_{r_1}(E_l) & -\mu_{r_2}(E_k) + \mu_{r_2}(E_l) \end{pmatrix} \begin{pmatrix} r_1 \\ r_2 \end{pmatrix} = \begin{pmatrix} \ln(A/A_0) \\ \ln(B/B_0) \end{pmatrix} \tag{7}$$

with

$$\begin{aligned} A_0 &= I_0(E_i)/I_0(E_j) & A &= I(E_i)/I(E_j), \\ B_0 &= I_0(E_k)/I_0(E_l) & B &= I(E_k)/I(E_l), \end{aligned} \tag{8}$$

where r_1 and r_2 denote the thicknesses of the shielding layers, $I_0(E_i)$ and $I(E_i)$ denote the intensity of the E_i line detected without and with shielding layers, respectively, and $\mu_{r_1}(E_i)$ and $\mu_{r_2}(E_i)$ denote the absorption coefficient of the first and second shielding layers for the E_i line. For solving the unknown thicknesses of the shielding layers, four energy lines, i.e., 122, 244, 344 and 778 keV, are adopted. The intensity I and I_0 for these energy lines are obtained from the detected gamma-ray spectrum, while the absorption coefficients for the copper and aluminum are obtained by the Monte Carlo simulation and are shown in Table 4.

Using the experimental intensities and simulated absorption coefficients, the thicknesses of copper and aluminum layers are solved by searching the nonnegative solution for Eq. 7 and are shown in Table 5. An even larger deviation appears for both the copper layer and aluminum layer thicknesses in the gamma-ray absorption results in comparison with the inverse results. Except for the same reason as the IRT-DEGL model, there are also several factors affecting the calculation precision for the gamma-ray absorption method. As the case of one shielding layer, only four energy lines used in the gamma-ray absorption method are not enough for the accurate estimation of the layer thicknesses, and the additional treatment of the absorption coefficient and the detected spectrum without shielding layer may also introduce more numerical errors. Furthermore, for the case of two shielding layers, instead of the simple analytic expression for the one-layer case, one has to deal with the nonnegative solution of matrix equation, which would possibly introduce a larger numerical error, especially for the ill-condition case. For the multi-layer case, one has to deal with multi-dimension matrix equations, which will necessarily bring in a notable numerical error.

In contrast, the IRT-DEGL model solves the unknown layer thicknesses by iteratively adjusting the hypothetical transport model to match the measured spectrum, which indicates that the numerical solution for the matrix equation is avoided and does not introduce the additional parameters, e.g., absorption coefficients in the gamma-ray absorption method, which can also help to avoid bringing in unnecessary numerical errors. Besides, the IRT-DEGL model is more general in its applications, for instance,

Table 4 Absorption coefficients of Cu and Al obtained with the Monte Carlo simulation

E (keV)	122	244	344	778
μ_{Cu} (cm ⁻¹)	2.523	1.034	0.856	0.569
μ_{Al} (cm ⁻¹)	0.395	0.363	0.242	0.163

Table 5 Comparison between the results from the gamma-ray absorption method and the inverse transport method

	Absorption method		IRT-DEGL model	
	Cu	Al	Cu	Al
r (cm)	0.373	0.200	0.316	0.534
$ \delta r/r $	21.10%	61.31%	2.60%	6.32%

solving for one-dimension or multi-dimension shielding layers is basically the same except for more shielding layers added into the photon transport model in simulation, and can be easily applied to study the source system with more unknown properties in the same framework, for example, both density and thickness of the shielding layer are unknown.

4 Summary and conclusion

In summary, an inverse radiation transport model based on an enhanced differential evolution algorithm with global and local neighborhoods (IRT-DEGL) is developed for identifying the unknown shielding layer thickness. The framework is briefly introduced with the key formalism on handling the enhanced differential evolution algorithm. The IRT-DEGL code is verified by using both the simulated and detected gamma-ray spectra. Using the simulated gamma-ray spectra, the numerical precision of the IRT-DEGL code is evaluated for two multilayered source/shield systems, where the calculated thicknesses of the multi-shielding layers are the same with the real values up to 0.001 cm. Using the detected gamma-ray spectra after optimization of the dead layer thickness for the HPG detector crystal by detection efficiency calibration, the unknown thicknesses for the one shielding layer and two shielding layers are investigated in the IRT-DEGL method. It is found that in comparison with traditional gamma-ray absorption method, the IRT-DEGL method can consider more gamma-ray spectrum characteristics and avoid the additional treatments that may introduce numerical errors, e.g., the absorption coefficient and ill-conditioned equations, and therefore, a much more accurate result can be provided. Furthermore, because of the tractability and generality of the IRT-DEGL method for applications, the IRT-DEGL model may have great potential to be applied for the complicated systems.

Acknowledgements The authors would like to acknowledge Ming-Cong Lan, Xiao-Jun Dang and Wei-Bo He for the discussions during the whole work.

References

- G.R. Gilmore, *Practical Gamma-Ray Spectrometry*, 2nd edn. (Wiley, Chichester, 2008). doi:[10.1002/9780470861981](https://doi.org/10.1002/9780470861981)
- N.J. McCormick, Inverse radiative transport problems: a review. *Nucl. Sci. Eng.* **112**, 185–198 (1992)
- Y.Y. Huang, Y.Y. Chen, D.F. Tian et al., γ -Ray self-absorption of cylindrical fissile material. *Nucl. Sci. Tech.* **16**(1), 17–24 (2005)
- C.Y. Wu, D.F. Tian, Y.Y. Cheng et al., Gamma ray absorption of cylindrical fissile material with dual shields. *Nucl. Sci. Tech.* **16**(5), 266–272 (2005)
- A.F. Iyudin, V. Burwitz, J. Greiner et al., Gamma-ray absorption method (GRAM) application to the identification of egret unidentified sources. *Astron. Astrophys.* **468**, 919–926 (2007). doi:[10.1051/0004-6361:20066890](https://doi.org/10.1051/0004-6361:20066890)
- L.P. Zhang, L.Q. Wu, M.F. Wei, Study on the gamma passive analysis for the thickness of two layer shield materials. *Nucl. Electr. Detect. Technol.* **330**(45), 322–324 (2015)
- J. Mattingly, D.J. Mitchell, A framework for the solution of inverse radiation transport problems. *IEEE Trans. Nucl. Sci.* **57**, 3734–3743 (2010). doi:[10.1109/NSSMIC.2008.4774636](https://doi.org/10.1109/NSSMIC.2008.4774636)
- S.J. Norton, A general nonlinear inverse transport algorithm using forward and adjoint flux computations. *IEEE Trans. Nucl. Sci.* **44**, 153–162 (1997). doi:[10.1109/23.568797](https://doi.org/10.1109/23.568797)
- J.A. Favorite, K.C. Bledsoe, Using the Levenberg–Marquardt method for the solution of inverse transport problems. *Trans. Am. Nucl. Soc.* **95**, 527 (2006)
- K.C. Bledsoe, J.A. Favorite, T. Aldemir, Application of the differential evolution method to solving inverse transport problems. *Nucl. Sci. Eng.* **169**, 208–211 (2011)
- K.C. Bledsoe, J.A. Favorite, T. Aldemir, Using the Levenberg–Marquardt method for solutions of inverse transport problems in one- and two-dimensional geometries. *Nucl. Technol.* **176**, 106–126 (2011)
- J.C. Armstrong, J.A. Favorite, Identification of unknown interface locations in a source/shield system using the mesh adaptive direct search method. *Trans. Am. Nucl. Soc.* **107**, 375–377 (2012)
- K.C. Bledsoe, J.A. Favorite, Using the Marquardt method for solution of inverse transport problems in two-dimensional cylinders. *Trans. Am. Nucl. Soc.* **98**, 591 (2008)
- J. Mattingly, D.J. Mitchell, Implementation and testing of a multivariate inverse radiation transport solver. *Appl. Radiat. Isot.* **70**, 1136–1140 (2012). doi:[10.1016/j.apradiso.2011.10.020](https://doi.org/10.1016/j.apradiso.2011.10.020)
- J. Mattingly, D.J. Mitchell, L.T. Harding, Experimental validation of a coupled neutron photon inverse radiation transport solver. *Nucl. Instrum. Methods Phys. Res. Sect. A* **652**, 537–539 (2011). doi:[10.1016/j.nima.2011.01.139](https://doi.org/10.1016/j.nima.2011.01.139)
- K.C. Bledsoe, J.A. Favorite, T. Aldemir, A comparison of the covariance matrix adaptation evolution strategy and the Levenberg–Marquardt method for solving multidimensional inverse transport problems. *Ann. Nucl. Eng.* **38**, 897–904 (2011). doi:[10.1016/j.anucene.2010.09.014](https://doi.org/10.1016/j.anucene.2010.09.014)
- K.C. Bledsoe, Inverse methods for radiation transport. Ph.D. Thesis, Ohio State University (2009)
- S. Das, A. Abraham, U.K. Chakraborty et al., Differential evolution using a neighborhood-based mutation operator. *IEEE Trans. Evol. Comput.* **3**, 526–553 (2009). doi:[10.1109/TEVC.2008.2009457](https://doi.org/10.1109/TEVC.2008.2009457)
- P.N. Suganthan, Differential evolution algorithm: recent advances. *Lect. Notes Comput. Sci.* **7505**, 47–56 (2012)
- Mcnp-a general Monte Carlo n-particle transport code, version 5. X-5 Monte Carlo Team, LA-CP-03-0245, Los Alamos National Laboratory (2003)
- M. Garcia-Talavera, H. Neder, M.J. Daza et al., Towards a proper modeling of detector and source characteristics in Monte Carlo simulations. *Appl. Radiat. Isot.* **52**, 777 (2000). doi:[10.1016/S0969-8043\(99\)00244-4](https://doi.org/10.1016/S0969-8043(99)00244-4)
- D. Budjas, M. Heisel, W. Maneschg et al., Optimisation of the mc model of a p type Ge spectrometer for the purpose of efficiency determination. *Appl. Radiat. Isot.* **67**, 706 (2009). doi:[10.1016/j.apradiso.2009.01.015](https://doi.org/10.1016/j.apradiso.2009.01.015)